Journal of Biomechanics 137 (2022) 111097

Contents lists available at ScienceDirect

Journal of Biomechanics

journal homepage: www.elsevier.com/locate/jbiomech

Modelling fore- and hindlimb peak vertical force differences in trotting horses using upper body kinematic asymmetry variables

Christoffer Roepstorff [a,*], Annik Imogen Gmel [a,b], Samuel Arpagaus [a], Filipe Manuel Serra Bragança [c], Elin Hernlund [d], Lars Roepstorff [d], Marie Rhodin [d], Michael Andreas Weishaupt [a]

[a] Equine Department, Vetsuisse Faculty, University of Zurich, Winterthurerstrasse 260, CH-8057 Zurich, Switzerland
[b] Agroscope – Swiss National Stud Farm, Les Longs-Prés, CH-1580 Avenches, Switzerland
[c] Department of Clinical Sciences, Faculty of Veterinary Medicine, Utrecht University, Yalelaan 112-114, NL-3584 CM Utrecht, the Netherlands
[d] Department of Anatomy, Physiology and Biochemistry, Swedish University of Agricultural Sciences, Uppsala, Sweden

ARTICLE INFO

Keywords:
Equine kinematics
Kinetics
Lameness
Motion capture
Time–frequency analysis

ABSTRACT

Differences in peak vertical ground reaction forces (dFz_{peak}) between contralateral forelimbs and hindlimbs are considered the gold standard for quantifying weight-bearing lameness. However, measuring kinematics for the same purpose is more common and practical. Vertical movement asymmetries (VMA) of the horse's upper body have previously been correlated to fore- and hindlimb lameness. But the combined response of head, withers and pelvis VMA to fore- and hindlimb dFz_{peak} has not yet been thoroughly investigated. Deriving the kinetic responses from kinematics would help the interpretation and understanding of quantified weight-bearing lameness.

In this retrospective study, 103 horses with a wide range of fore- and hindlimb dFz_{peak} had been trotted on a force-measuring treadmill synchronized with an optical motion capture system. VMA of the head, withers and pelvis as well as dFz_{peak} were extracted. Multiple linear mixed models and linear regressions of kinematic variables were used to model the dFz_{peak}. It was hypothesised that all included VMA would have a significant influence on the dFz_{peak} outcome variables.

The results showed a complex relationship between VMA and dFz_{peak} where both amplitude and timing of the VMA were of importance. On average, the contribution percentage of VMA to fore/hind dFz_{peak} were 66/34% for head, 76/24% for withers and 33/67% for pelvis. The linear regressions for the fore/hindlimb models achieved mean measurement root mean squared errors of 0.83%/0.82% dFz_{peak}. These results might help determine the clinical relevance of upper body VMA and distinguish between primary fore, hind, ipsilateral and diagonal weight-bearing lameness.

1. Introduction

Measuring horses in motion for objective lameness evaluation has become increasingly more accessible using either optical motion capture systems (OMC) or inertial measurement units (IMU) (Bosch et al., 2018; Keegan, 2007; Serra Bragança et al., 2018). Kinematic analysis of trotting horses has shown that the vertical movement asymmetries (VMA) of the head, withers and pelvis can be used as indicators of weight-bearing lameness. Typically, head and withers VMA have been associated with forelimb lameness and pelvis VMA with hindlimb lameness (Buchner et al., 1996; Peloso et al., 1993). But ancillary kinematic adaption strategies have also been observed. For example, horses with an induced forelimb lameness exhibited a pelvis VMA indicating a contralateral hindlimb lameness, similarly, when a hindlimb lameness was induced, the head VMA indicated an ipsilateral forelimb lameness while the withers indicated a contralateral forelimb lameness (Kelmer et al., 2005; Rhodin et al., 2018; Uhlir et al., 1997). See Table 1 for a list of abbreviations used throughout the paper.

Although kinematic measurements are more commonplace, vertical ground reaction force measurements remain the gold standard for quantifying weight-bearing lameness. Results have shown that in horses, inducing pain in one limb caused a reduction of peak vertical ground reaction force (Fz_{peak}) in that limb (Ishihara et al., 2005; Merkens and Schamhardt, 1988a, 1988b). Inducing lameness in a forelimb during trot

* Corresponding author.
E-mail address: christoffer.roepstorff@uzh.ch (C. Roepstorff).

https://doi.org/10.1016/j.jbiomech.2022.111097
Accepted 11 April 2022
Available online 15 April 2022

Table 1
List of abbreviations and mathematical quantities.

Abbreviation/ Quantity	Description
OMC	Optical Motion Capture
	Measurement system using cameras and reflective markers to measure movements
IMU	Inertial Measurement Unit
VMA	Vertical Movement Asymmetry
	A general term for any type of variable used for quantifying vertical movement asymmetries within a stride. Examples include, PD_{min}, HD_{max} and odd harmonic components.
Fz_{peak}	Peak vertical force
	The maximum vertical force measured for one limb and one step. Measured in Newtons.
Fz_{peakxx}	Peak vertical force for limb **xx**
	Limbs are specified as front left (fl), front right (fr), hind left (hl) and hind right (hr). For example, Fz_{peakfl} would indicate the peak vertical force of the left forelimb.
dFz_{peak}	Peak vertical force difference
	Difference between contralateral limb Fz_{peak} normalised by the sum of the same contralateral Fz_{peak} and multiplied by 100. Measured in %.
dFz_{peakx}	Peak vertical force difference between contralateral limbs **x**
	The limb pairs are specified as either forelimb (f) or hindlimb (h). For example, dFz_{peakh} would indicate a hindlimb dFz_{peak}.
D_{min}	Minimum difference in vertical position
	Difference between the minimums in vertical position occurring during one stride.
D_{max}	Maximum difference in vertical position
	Difference between the maximums in vertical position occurring during one stride.
$\boldsymbol{X}$	Collection of vertical movement trajectories $\boldsymbol{X} = (H, W, P)$,
	where the H = head, W = withers and P = pelvis.
x	Single trajectory of vertical movement
	Used to indicate the vertical movement of one of the three kinematic trajectories. Either the head ($x = H$), withers ($x = W$) or pelvis ($x = P$).
$xD_{\min} xD_{max}$	Minimum/maximum difference in vertical position for x For example, the minimum difference in vertical head movement would be labelled HD_{min} and the maximum difference in pelvis vertical movement would be labelled PD_{max}.
n	Harmonic component number The number and multiplier used for describing the harmonic components of strides, $n = 1, 2, 3$.
x_n	Harmonic component number n for x
	Used to describe a stride's vertical movement harmonic component. For example, H_1 would indicate the first harmonic component of the head vertical movement for one stride.
$\ddot{x}_n$	Harmonic component number n for the acceleration x
	Used to describe a stride's vertical acceleration harmonic component. For example, $\ddot{P}_3$ would indicate the third harmonic component of the pelvis vertical acceleration for one stride.
a_{xn}	Amplitude of harmonic component n for vertical position x For example, a_{H1} would indicate the amplitude of the first component of a stride of head vertical movement.
$\widehat{a}_{xn}$	Amplitude of harmonic component n for vertical acceleration x For example, $\widehat{a}_{W1}$ would indicate the amplitude of the first component of a stride of withers vertical acceleration.
φ_{xn}	Phase of harmonic component n for vertical position x For example, φ_{P3} would indicate the phase of the third component of a stride of pelvis vertical movement.
ω	Stride angular frequency
	The fundamental angular frequency of a stride associated with the harmonic components. Calculated as $w = 2\pi f$, where f is the stride frequency
β_A	Mixed linear model coefficients for amplitudes
β_φ	Mixed linear model coefficients for phases
RMSE	Root Mean Squared Error
R^2	R-squared

also resulted in a compensatory Fz_{peak} reduction in the ipsilateral hindlimb (Serra Bragança et al., 2020a; Weishaupt et al., 2006). In contrast, when a hindlimb lameness was induced, no compensatory Fz_{peak} reduction was observed (Weishaupt et al., 2004). See Fig. 1 for examples from this study. Kinetic asymmetries can be quantified as differences between left and right Fz_{peak} (dFz_{peak}) for both fore- (dFz_{peakf}) and hindlimbs (dFz_{peakh}).

The quantification of VMA can be done in different ways. One approach is to calculate the minimum and maximum vertical position differences (D_{min}, D_{max}) between left and right steps (Buchner et al., 1996; Keegan et al., 2000; Kramer et al., 2000; Rhodin et al., 2018). Although acceleration and forces are more directly connected ($F = ma$), research studies have more frequently used position to calculate VMA (Serra Bragança et al., 2018). It is also possible to use Fourier analysis to extract harmonic components from upper body vertical movement. The first odd component can then be used to describe the VMA of the stride as a function of its amplitude and phase (Audigié et al., 2002; Peham et al., 1996). Higher orders of odd harmonics have been analysed using a single girth-mounted IMU, but not with regards to head, withers and pelvis VMA (Halling Thomsen et al., 2010). The 3rd harmonic of pelvis rotation signals has also been used to extract movement features that were difficult to detect in raw time series data (Roepstorff et al., 2021). Incorporating higher-order harmonics, specifically the 3rd component, in the VMA analysis and using acceleration instead of position could possibly uncover information related to weight-bearing asymmetries that have not yet been studied.

The VMA of the head, withers and pelvis all appear to be involved in both fore and hindlimb weight-bearing lameness. But so far, no attempt has been made to investigate the combined response of these three VMA to changes in dFz_{peakf} and dFz_{peakh}. Distinguishing between primary forelimb, hindlimb, ipsilateral, diagonal and bilateral weight-bearing lameness is a complex problem when interpreting kinematic data. A deeper understanding of how kinetics and kinematics interact could reduce this complexity and benefit the clinical applicability of kinematic lameness assessments.

This study aimed to investigate the interaction between vertical kinetic and kinematic asymmetries through modelling dFz_{peakf} and dFz_{peakh} in trotting horses as multiple linear regressions and mixed linear models of upper body VMA. We hypothesised that the VMA from head, withers and pelvis would all have a significant influence on the outcome variables dFz_{peakf} and dFz_{peakh}. Furthermore, we hypothesised that including the 3rd harmonic in the VMA and using acceleration instead of position would improve the model fits.

2. Materials and methods

2.1. Horses

A total of 103 horses were included in the study, aggregated from three different projects. In project 1 (P1), ten warmblood horses were

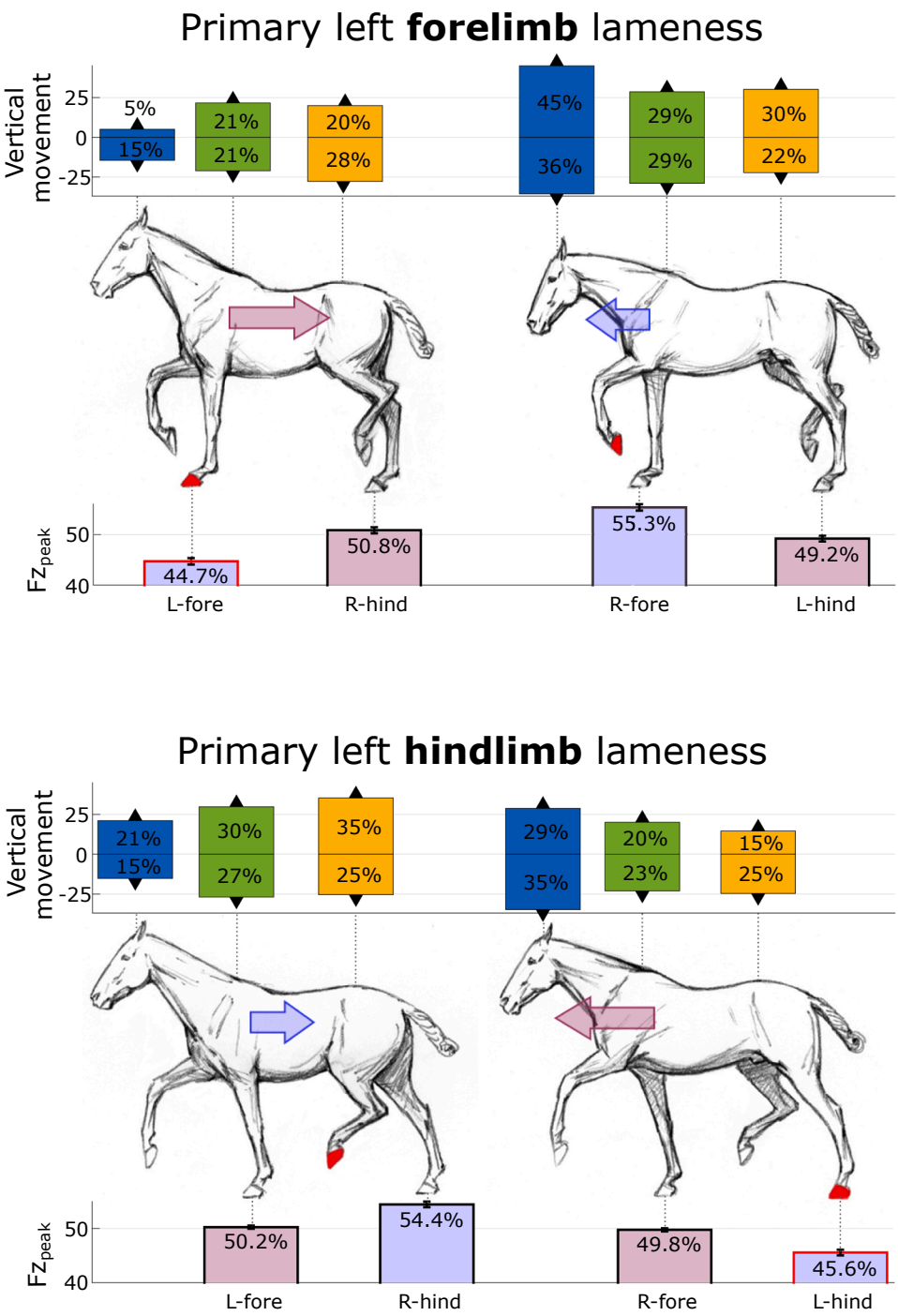

Fig. 1. Kinetic and kinematic symmetry examples of induced left fore- and hindlimb lamenesses at trot. One stride with its two diagonal limb stance phases (steps) are depicted for the two lamenesses. Head (blue), withers (green) and pelvis (yellow) indicate the mean up and down movement per step presented as the percentage of the total movement per stride for each of the three movements. Mean peak vertical forces (Fz_{peak}) are displayed as percent of total limb pair (fore and hind) Fz_{peak}. The red hoof indicates the lame limb and the arrows the diagonal weight-shift. The left forelimb lameness exhibits a left fore Fz_{peak} deficit and a secondary ipsilateral hindlimb Fz_{peak} deficit. Head and withers movement appears to match with the forelimb Fz_{peak} deficit with relatively less movement during the left fore step. Pelvis movement does not appear to match with the secondary left hindlimb Fz_{peak} deficit, instead showing relatively more movement during the left hind step. The hindlimb lameness exhibits a left hind Fz_{peak} deficit and an almost symmetrical forelimb Fz_{peak} distribution. Pelvis movement appears to match with the hind Fz_{peak} deficit with relatively less movement during the left hind step. Head movement is relatively smaller during the ipsilateral forelimb step and withers movement is smaller during the diagonal forelimb step.

trotted while lameness was induced using a sole pressure model. All four limbs were induced one limb at the time, with different degrees of pressure for each measurement, resulting in 179 measurements. The project has previously been described by Rhodin et al., 2018. In project 2 (P2), 24 Franches-Montagnes stallions deemed as clinically sound by an experienced clinician (M.A.W.) were trotted in multiple measurements at different speeds (3.3–6.6 m/s), resulting in 126 measurements. In project 3 (P3), 69 horses, non-lame according to their owners, were trotted in multiple measurements at different speeds (2.8–6.1 m/s), resulting in 426 measurements. In P2 and P3 the speed was incrementally increased between measurements, starting at the horses lowest possibly trotting speed and ending at the highest possible speed before breaking into canter. The horses were of various breeds, with the majority being Warmbloods; see supplementary material for a list of included breeds. The three projects were performed according to the animal health and welfare regulations under permits ZH51/2013–5054 (P1), VD3164 (P2) and ZH003/17–28698 (P3).

2.2. Measurements

All horses were fitted with reflective markers on the head (on, or close to, the poll), withers (T6-T8) and pelvis (S1) as has been previously described (Rhodin et al., 2018). All measurements lasted 20 s and were performed on an instrumented treadmill measuring the vertical ground reaction forces of all four limbs at 512 Hz (P1) and 480 Hz (P2, P3) (Weishaupt et al., 2002). Simultaneous and synchronised kinematics

were measured using an OMC system (Qualisys AB, Gothenburg, Sweden), consisting of 10 Oqus 300 cameras sampling at 256 Hz (P1) and 10 Oqus 7 + at 240 Hz (P2, P3). The 731 measurements were selected such that they had at least 20 strides in steady-state trot resulting in 18 995 strides in total.

2.3. Data processing

Kinetic data were analysed using the HP2 software (University of Zurich, Zurich, Switzerland). Strides were defined as segments delimited by consecutive left forelimb hoof-on events. For each stride, dFz_{peak} between the left (l) and right (r), fore- and hindlimbs were calculated as,

$$dFz_{peakf} = \frac{Fz_{peakfl} - Fz_{peakfr}}{Fz_{peakfl} + Fz_{peakfr}} * 100 \quad (1)$$

$$dFz_{peakh} = \frac{Fz_{peakhl} - Fz_{peakhr}}{Fz_{peakhl} + Fz_{peakhr}} * 100 \quad (2)$$

Kinematics were captured using Qualisys Track Manager (QTM, Qualisys AB, Gothenburg, Sweden). Custom made Matlab (MATLAB, 2020b, The MathWorks Inc, Natick, USA) scripts were used for further processing of both kinetic and kinematic data. The vertical position of the head (H), withers (W) and pelvis (P), were filtered using a 4th order Butterworth filter with a cut-off frequency adapted to the stride frequency (0.7*$stridefrequency$) (Serra Bragança et al., 2020b). Each trajectory was subsequently split into strides using the kinetic segmentation from HP2. Modelling and statistics were done using the Statistics and Machine Learning Toolbox and circular statistics were calculated using the Circular Statistics Toolbox in Matlab (Berens, 2015).

2.4. Feature extraction

The D_{min} and D_{max} were calculated for each trajectory and stride in $\boldsymbol{X} = (H, W, P)$ and four feature sets were created to enable the comparison between, combing head, withers and pelvis VMA versus, using only the head, pelvis or the head and pelvis combination,

$$\boldsymbol{f}_{D1} = (HD_{max}, HD_{min}, WD_{max}, WD_{min}, PD_{max}, PD_{min}) \quad (3)$$

$$\boldsymbol{f}_{D2} = (HD_{max}, HD_{min}, PD_{max}, PD_{min}) \quad (4)$$

$$\boldsymbol{f}_{D3} = (HD_{max}, HD_{min}) \quad (5)$$

$$\boldsymbol{f}_{D4} = (PD_{max}, PD_{min}) \quad (6)$$

where the D_{min} were defined as the minimum vertical position occurring during the right limb stance phase minus the minimum occurring during the left limb stance phase (HD_{min}, WD_{min} during forelimb and PD_{min} during hindlimb stance), as has been previously

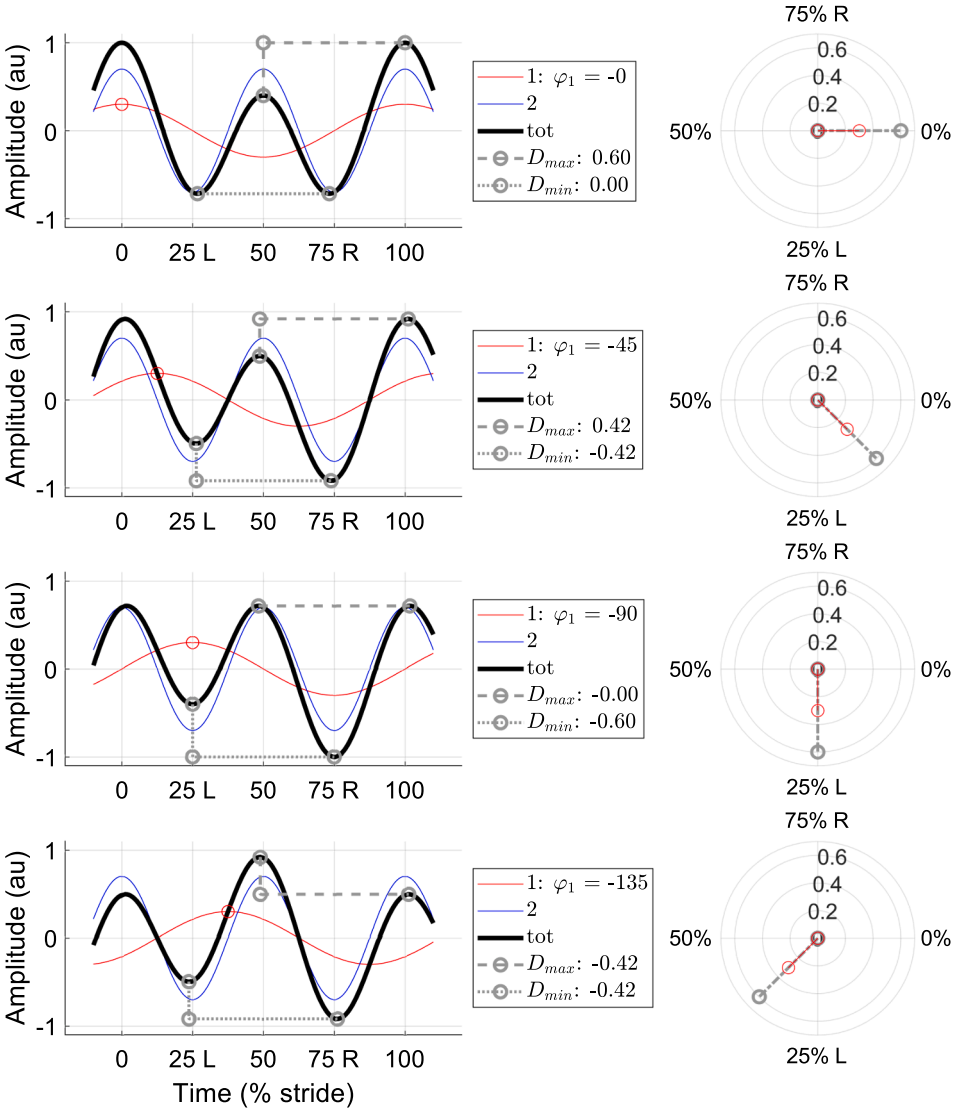

Fig. 2. Four theoretical examples of asymmetric movement and their polar representation, for one stride left (L) to right (R) step, based on the two-component harmonic model. The examples represent four different timings, or phases (φ), of the first asymmetric component (red). The blue line indicates the second component. The thicker black line is the superposition of the two components (red and blue) and the dashed/dotted lines indicate the extracted D_{max} and D_{min}. At trot, mid-stance occurs approximately at 25% and at 75% for the left and the right limb respectively. The zero phase is defined in relation to the second symmetric component (blue). The polar graphs shows that D_{max} and D_{min} (grey) approximate a scaled version of the information contained in the amplitude and phase of the asymmetric sinusoid (red).

described (Keegan et al., 2000; Kramer et al., 2000). The D_{max} were defined as the maximum vertical position occurring after a right stance phase minus the maximum occurring after a left stance phase (HD_{max}, WD_{max} after forelimb and PD_{min} after hindlimb stance). This definition produces the opposite sign of the conventional definition, see Fig. 2 (Kramer et al., 2000).

The first three harmonic components were extracted for each stride and trajectory in $\boldsymbol{X}$ using a segmented FFT approach, as has been previously described (Roepstorff et al., 2021). These components, $(H_n, W_n, P_n)|_{n=1,2,3}$, could be described in terms of an amplitude (a_{Hn}, a_{Wn}, a_{Pn}), the fundamental angular frequency ($\omega = 2\pi f, f =$ stride frequency) and a phase ($\varphi_{Hn}, \varphi_{Wn}, \varphi_{Pn}$) where $n = 1, 2, 3$. All component phases were shifted to be relative to the second component zero phase,

$$\varphi_{xn} \overset{\text{def}}{=} \varphi_{xn} - \frac{n\varphi_{x2}}{2} \tag{7}$$

In the two-component harmonic model, the theoretical connection between the first component and the D_{max} and D_{min} is illustrated in Fig. 2. Since the third component is also asymmetric over a stride it was plausible to assume that it might be correlated to weight-bearing lameness in the same way as the first component is (Audigié et al., 2002; Peham et al., 1996). The analytical nature of the harmonic representation enabled a way to describe a single stride with three components for each trajectory in $\boldsymbol{X}$,

$$x(t) = Re\left(\sum_{n=1}^{3} a_{xn} e^{i(n\omega t + \varphi_{xn})}\right) + \varepsilon \Big|_{x=H,W,P} \tag{8}$$

where ε is the error containing information on offset, noise and any unexplained harmonic content. This analytical representation could be differentiated twice with respect to time without any of the drawbacks typically associated with differentiating sampled data,

$$\ddot{x}(t) = Re\left(\sum_{n=1}^{3} -a_{xn}(n\omega)^2 e^{i(n\omega t + \varphi_{xn})}\right) + \varepsilon'' \Big|_{x=H,W,P} \tag{9}$$

From equation (9) the acceleration amplitude can be extracted and defined as,

$$\hat{a}_{xn} = -a_{xn}(n\omega)^2 \tag{10}$$

illustrating how the $\hat{a}_{xn}$ is the negative a_{xn} scaled by the square of the component frequency. By extracting the real and imaginary parts of the first and third components when equations (8) and (9) were evaluated at $t = 0$, three more feature sets were created,

$$\boldsymbol{f}_{C1} = \left(Re\left(a_{xn}(n\omega)^2 e^{i\varphi_{xn}}\right), Im\left(a_{xn}(n\omega)^2 e^{i\varphi_{xn}}\right)\right)\Big|_{\substack{x=H,W,P \\ n=1,3}}$$

$$= \left(\ddot{x}_{nre}, \ddot{x}_{nim}\right)\Big|_{\substack{x=H,W,P \\ n=1,3}}$$

$$= \left(\ddot{H}_{1re}, \ddot{H}_{1im}, \ddot{H}_{3re}, \ddot{H}_{3im}, \ddot{W}_{1re}, \ddot{W}_{1im}, \ddot{W}_{3re}, \ddot{W}_{3im}, \ddot{P}_{1re}, \ddot{P}_{1im}, \ddot{P}_{3re}, \ddot{P}_{3im}\right) \tag{11}$$

$$\boldsymbol{f}_{C2} = \left(Re\left(a_{xn}e^{i\varphi_{xn}}\right), Im\left(a_{xn}e^{i\varphi_{xn}}\right)\right)\Big|_{\substack{x=H,W,P \\ n=1,3}}$$

$$= \left(x_{nre}, x_{nim}\right)\Big|_{\substack{x=H,W,P \\ n=1,3}}$$

$$= \left(H_{1re}, H_{1im}, H_{3re}, H_{3im}, W_{1re}, W_{1im}, W_{3re}, W_{3im}, P_{1re}, P_{1im}, P_{3re}, P_{3im}\right) \tag{12}$$

$$\mathbf{f}_{C3} = \left(\mathrm{H_{1re}}, \mathrm{H_{1im}}, \mathrm{W_{1re}}, \mathrm{W_{1im}}, \mathrm{P_{1re}}, \mathrm{P_{1im}}\right) \tag{13}$$

note that the negative sign was removed from the acceleration components in $\boldsymbol{f}_{C1}$. This was done in order to provide amplitude signs consistent with all the other feature sets.

2.5. Linear mixed models

Seven different linear mixed models were created for both dFz_{peakf} and dFz_{peakh} with independent variables from the feature sets $\boldsymbol{f}_{C1-C3}$ and $\boldsymbol{f}_{D1-D4}$. Random intercepts $\boldsymbol{U}$ were created by grouping samples by individual horse and movement speed, see Table 2. The independent variables were standardised, by first subtracting their mean values and then dividing by their standard deviations, before the modelling. Independent variables in all feature sets were tested for collinearity using a Belsley collinearity test (Belsley et al., 1980). Significant difference of fit between models was tested using a simulated log likelihood test (50 simulations, $\alpha = 0.05$) and AIC model selection using Akaike weights. The feature pairs $(xD_{max}, xD_{min})|_{x=H,W,P}$, $(x_{1re}, x_{1im})|_{x=H,W,P}$ and $(x_{3re}, x_{3im})|_{x=H,W,P}$, can all be considered components of asymmetry. Because of this the model coefficients belonging to these pairs were selected to be transformed to polar coordinates for the best fitting models from feature families $\boldsymbol{f}_C$ and $\boldsymbol{f}_D$. This enabled coefficient analysis of amplitude (β_A) and phase (β_φ), and their respective confidence intervals. Simulated asymmetry with amplitude 1, spanning all phases were fed in the models with the best fit. The simulated response for each feature pair, as well as their respective distribution between fore and hind responses $\left(\frac{fore}{fore+hind}, \frac{hind}{fore+hind}\right)$, were visualised in polar graphs to analyse the coefficient responses.

2.6. Linear regression

The total data set of strides was randomly split into training and test data sets where ~30% of the horses from each project (P1, P2, P3) were included in the test data set and the rest in the training data set. To evaluate the practical application of the mixed models investigated, the same designs were used in linear regression models, which were trained and cross-validated using five-folds and finally tested. The best models from feature families $\boldsymbol{f}_C$ and $\boldsymbol{f}_D$ were selected based on the mean RMSE values from the cross-validation. When tested, the RMSE and R^2 were calculated for the modelled strides and for the modelled mean stride per measurement.

3. Results

3.1. Linear mixed models

Model comparisons of fit are presented in Table 3. Models C_{1f} and C_{1h} produced significantly ($\alpha = 0.05$) better fits compared to all the other models. Models C_{2f} and C_{2h} had a significantly better fit compared to models D_{1f} and D_{1h}. Models D_{1f} and D_{1h} had significantly better fits than models C_{3f} and C_{3h}, where the third component variables were excluded. Hindlimb model D_{2h}, excluding the withers asymmetry

Table 2
Model design for the linear mixed models. Relative peak vertical force differences (dFz_{peak}) between fore (f) and hindlimb (h) pairs, measured in percent, were modelled as linear combinations of independent variables from seven different feature sets. Random intercepts ($\boldsymbol{U}$) were created by grouping samples by individual horse and movement speed. The regression models used the same design excluding the random intercept.

Model name	Model design (y = f, h)
C_{1y}	$dFz_{peaky} = \boldsymbol{f}_{C1}\beta + \boldsymbol{U}\boldsymbol{\gamma} + \varepsilon$
C_{2y}	$dFz_{peaky} = \boldsymbol{f}_{C2}\beta + \boldsymbol{U}\boldsymbol{\gamma} + \varepsilon$
C_{3y}	$dFz_{peaky} = \boldsymbol{f}_{C3}\beta + \boldsymbol{U}\boldsymbol{\gamma} + \varepsilon$
D_{1y}	$dFz_{peaky} = \boldsymbol{f}_{D1}\beta + \boldsymbol{U}\boldsymbol{\gamma} + \varepsilon$
D_{2y}	$dFz_{peaky} = \boldsymbol{f}_{D2}\beta + \boldsymbol{U}\boldsymbol{\gamma} + \varepsilon$
D_{3y}	$dFz_{peaky} = \boldsymbol{f}_{D3}\beta + \boldsymbol{U}\boldsymbol{\gamma} + \varepsilon$
D_{4y}	$dFz_{peaky} = \boldsymbol{f}_{D4}\beta + \boldsymbol{U}\boldsymbol{\gamma} + \varepsilon$

Table 3
Model results and comparison for dFz_{peak}. The mixed linear models were compared both using a simulated least likelihood test ($\alpha = 0.05$) and the Aikake Criterion (AIC). The comparison column contains the models which had a significantly worse fit in the comparison. The best regression model was selected based on the smallest mean root mean squared error (RMSE) of the 5-fold cross validation on the training data set. The regression RMSE and R-squared (R^2) were calculated on both the individually modelled strides and the mean of strides per measurement for the test data set.

Fore - dFz_{peakf} (%)										
model	Linear mixed models				Regression models					
					Stride				Measurement	
	Comparison	R^2	RMSE	AIC	R^2 train	RMSE train	R^2 test	RMSE test	R^2 test	RMSE test
C_{1f}	$C_{2f}, C_{3f}, D_{1f}, D_{2f}, D_{3f}, D_{4f}$	0.88	0.82	48,460	0.75	1.16	0.73	1.18	0.82	0.83
C_{2f}	$C_{3f}, D_{1f}, D_{2f}, D_{3f}, D_{4f}$	0.87	0.84	49,535	0.74	1.20	0.72	1.20	0.81	0.85
C_{3f}	D_{2f}, D_{3f}, D_{4f}	0.85	0.90	51,801	0.70	1.28	0.70	1.23	0.81	0.87
D_{1f}	$C_{3f}, D_{2f}, D_{3f}, D_{4f}$	0.86	0.89	51,390	0.72	1.23	0.70	1.23	0.80	0.88
D_{2f}	D_{3f}, D_{4f}	0.78	1.09	59,450	0.53	1.60	0.41	1.73	0.48	1.42
D_{3f}	D_{4f}	0.75	1.17	61,901	0.48	1.69	0.36	1.81	0.42	1.50
D_{4f}	–	0.56	1.54	72,509	0.06	2.27	0.00	2.26	0.04	2.01
Hind - dFz_{peakh}(%)										
model	Linear mixed models				Regression models					
					Stride				Measurement	
	Comparison	R^2	RMSE	AIC	R^2 train	RMSE train	R^2 test	RMSE test	R^2 test	RMSE test
C_{1h}	$C_{2h}, C_{3h}, D_{1h}, D_{2h}, D_{3h}, D_{4h}$	0.92	0.79	47,243	0.83	1.15	0.81	1.12	0.85	0.82
C_{2h}	$C_{3h}, D_{1h}, D_{2h}, D_{3h}, D_{4h}$	0.91	0.83	49,046	0.80	1.24	0.80	1.16	0.84	0.84
C_{3h}	D_{3h}, D_{4h}	0.86	1.01	56,143	0.75	1.37	0.73	1.33	0.81	0.91
D_{1h}	$C_{3h}, D_{2h}, D_{3h}, D_{4h}$	0.88	0.95	53,827	0.76	1.33	0.74	1.30	0.80	0.94
D_{2h}	C_{3h}, D_{3h}, D_{4h}	0.88	0.95	53,863	0.74	1.39	0.71	1.38	0.76	1.03
D_{3h}	–	0.50	1.92	80,511	0.06	2.66	0.04	2.63	0.07	2.18
D_{4h}	D_{3h}	0.86	1.03	57,327	0.66	1.60	0.66	1.50	0.69	1.17

variables, had a better fit than C_{3h}.

Standardised coefficients transformed to polar coordinates, with their respective confidence intervals, for models C_{1f}, C_{1h}, D_{1f} and D_{1h} are presented in Table 4. The transformed model coefficients can be interpreted in the following way: when an input feature phase is equal to the model coefficient phase (β_φ), the response from that coefficient and feature is maximised. Analogously, an input phase-shifted by $\pm\pi$ radians to the coefficient phase will minimize the response. This meant that for each component variable pair (amplitude, phase) there were exactly two specific phase values where the summed response of the pair was zero, regardless of amplitude (see $H_1^{''}$ phases close to 0/360° and ± 180° in Fig. 3. β_A indicated the relative importance of each feature, as the dependent variables were standardised.

Within the two hindlimb models (C_{1h},D_{1h}) the pelvis features had the highest β_A values,$PD = 2.31$ and $P_1^{''} + P_3^{''} = 1.96 + 0.85$ and the withers features had the lowest β_A values,$WD = 0.11$ and $W_1^{''} + W_3^{''} = 0.18 + 0.23$. In the forelimb models (C_{1f}, D_{1f}), the withers features had the highest β_A values, $WD = 1.32$ and $W_1^{''} + W_3^{''} = 1.27 + 0.34$ and the pelvis features had the lowest values, $PD = 0.53$ and $P_1^{''} + P_3^{''} = 0.87 + 0.25$. The absolute distance between fore and hindlimb model coefficients β_φ were 2/7/8° for features $HD/H_1^{''}/H_3^{''}$, 71/107/96° for $WD/W_1^{''}/W_3^{''}$ and 15/39/134° for $PD/P_1^{''}/P_3^{''}$.

Fig. 3 illustrates the simulated responses for models C_{1f}, C_{1h}. The relative fore/hind contributions per feature and phase, including the mean responses over all phases, are presented in Fig. 4. The mean fore/hind response distribution for models C_{1f}/C_{1h} was $|H_1^{''}|$: 67/33%, $|W_1^{''}|$: 81/19%, $|P_1^{''}|$: 34/66%,$|H_3^{''}|$: 58/42%, $|W_3^{''}|$: 57/43% and $|P_3^{''}|$: 28/72%. Normalising components 1 and 3 by dividing by the sum of all β_A, and then adding them together, the summed contributions were, $|H_{1+3}^{''}|$: 66/34%, $|W_{1+3}^{''}|$: 76/24% and $|P_{1+3}^{''}|$: 33/67%. The mean fore/hind response distribution for models D_{1f}/D_{1h} was $|HD|$: 69/31%, $|WD|$: 92/8%, $|PD|$: 19/81%. Because the phase coefficients (β_φ) for the $H_1^{''}$ and $H_3^{''}$ variables were similar for the fore- and hindlimb models (only separated by 7° and 8°) the relative contribution to each dFz_{peak} was consistently 66% to the forelimb and 34% to the ipsilateral hindlimb. Conversely, the relative fore/hind contribution of withers and pelvis features were more susceptible to changes in β_φ. This unveiled some interesting effects, e.g., pelvic asymmetry occurring early/late during a step ($-4^\circ < \varphi_{P^{''}3} < 31^\circ$ and $176^\circ < \varphi_{P^{''}3} < -149^\circ$, roughly comparable to a curve with only a PD_{max}), resulted in a larger contribution to dFz_{peakf} than to the dFz_{peakh}, (Table 4 and Fig. 4).

Table 4
Model coefficients transformed to polar coordinates for models C_{1f}, C_{1h}, D_{1f} and D_{1h}. Features HD, WD, PD originate from the $D_{max/min}$ variables and $H''_{1/3}, W''_{1/3}, P''_{1/3}$ originate from the first (1) and third (3) harmonic acceleration components, for head (H) withers (W) and pelvis (P). Coefficients for amplitude (β_A) and Phase (β_φ) with 95% confidence intervals (CI) values were modelled using standardised variables. A feature input with phase equal to β_φ maximizes the contribution to dFz_{peak} (right limb weight bearing deficiency), conversely a feature phase equal to $\beta_\varphi \pm \pi$ minimizes the contribution to dFz_{peak} (left limb weight bearing deficiency).

	Fore (C_{1f}, D_{1f})						Hind (C_{1h}, D_{1h})					
Feature	β_A	β_A CI		β_φ (°)	β_φ CI		β_A	β_A CI		β_φ (°)	β_φ CI	
HD	1.19	1.17	1.22	102	101	103	0.54	0.52	0.56	100	97	102
WD	1.32	1.29	1.36	93	91	95	0.11	0.06	0.16	164	−179	135
PD	0.53	0.49	0.56	−101	−105	−98	2.31	2.28	2.34	−86	−86	−85
$H_1^{''}$	1.14	1.12	1.16	96	95	97	0.54	0.52	0.56	103	101	105
$W_1^{''}$	1.27	1.24	1.31	79	76	81	0.18	0.14	0.22	−174	−162	176
$P_1^{''}$	0.87	0.83	0.91	−121	−124	−119	1.96	1.93	1.99	−82	−83	−81
$H_3^{''}$	0.16	0.14	0.18	–32	−40	−24	0.12	0.10	0.14	−24	−35	−15
$W_3^{''}$	0.34	0.31	0.38	−71	−76	−65	0.23	0.20	0.27	25	18	32
$P_3^{''}$	0.25	0.23	0.28	−109	−116	−103	0.85	0.82	0.88	117	115	119

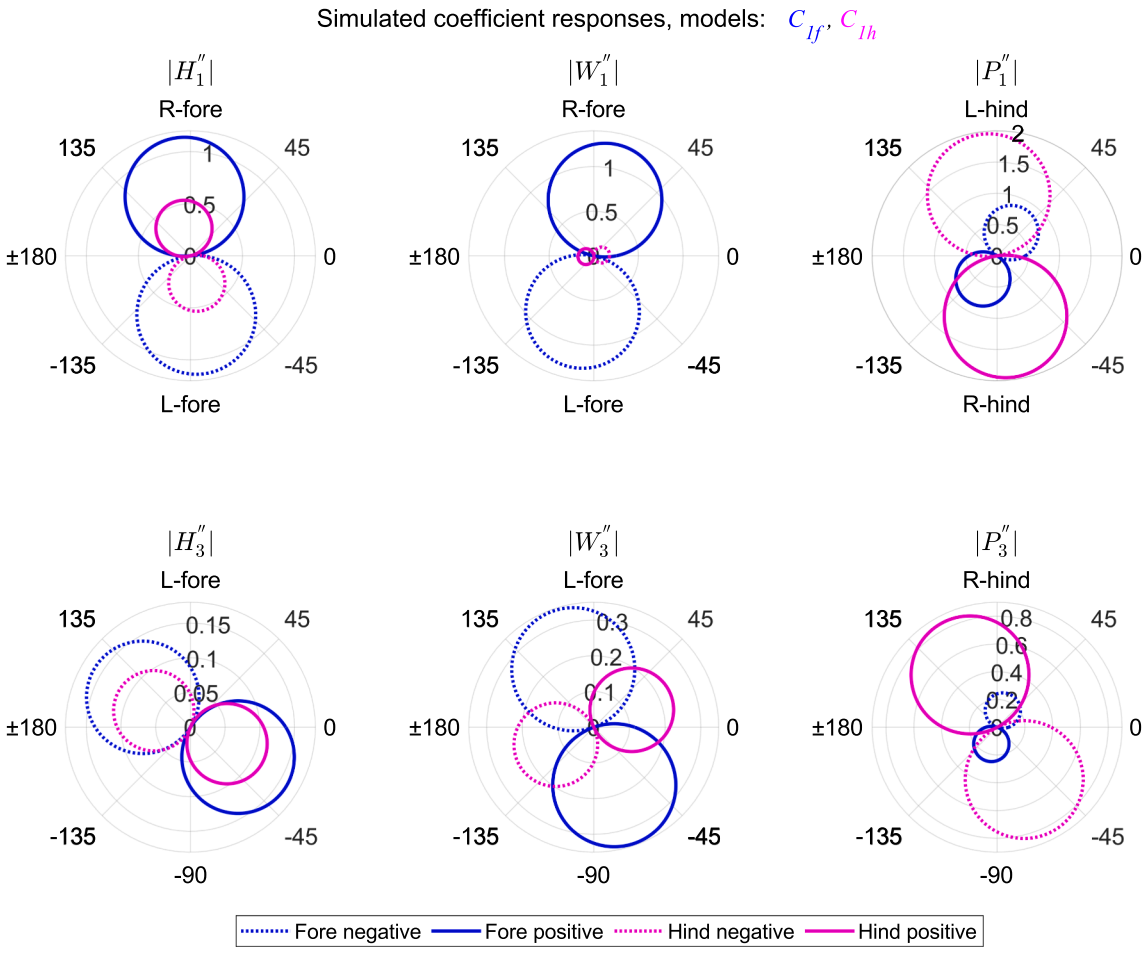

Fig. 3. Simulated coefficient responses for models C_{1f} (blue) and C_{1h} (magenta) when fed features with amplitude 1, spanning all phases ($-\pi < \varphi < \pi$). Model responses for component 1 (top) and 3 (bottom) for head (*H*), withers (*W*) and pelvis (*P*) appear dotted when indicating a negative dF_{zpeak} (left limb deficit) and solid for a positive dF_{zpeak} (right limb deficit). Contributions to dFz_{peakf} are depicted in blue and contributions to dFz_{peakh} are shown in magenta. The approximate time of midstance for each limb is indicated along the phase axis. Note how the head feature has similar phase responses for the fore and hindlimb models while withers and pelvis features have different fore/hind responses.

Simulated responses for D_{1f} and D_{1h}, bivariate distributions for the feature pairs and all mixed models can be found in the supplementary material.

The Belsley collinearity test showed no collinearity between the variables in the different feature sets that were above the suggested standard thresholds used by the Matlab function *collintest* (Sonnberger, 1989). The simulated log likelihood test and evaluation of the Akaike weights resulted in the same rating for all the linear mixed models.

3.2. Linear regression

Regression models C_{1f}/C_{1h} had the best training result with an RMSE of 1.16/1.15%, respectively. When tested, the two models achieved RMSE values of 1.18/1.12% on a stride-by-stride basis and 0.83/0.82% on a measurement mean basis. Models including features from all three trajectories (head, withers and pelvis) had training RMSE $\leq$ 1.33%, test stride-by-stride RMSE $\leq$ 1.3% and test measurement mean RMSE $\leq$ 0.94% (Table 3).

4. Discussion

4.1. Linear mixed models

We could not reject our hypothesis that all VMA would have a significant influence on the modelled dF_{zpeak}. However, in the case of dF_{zpeakh} the relative importance of withers VMA were small. We also could not reject our hypothesis that the third harmonic component was significantly correlated with dF_{zpeak}. Harmonic components can be derived from the concept of a simple spring-mass model, which is only valid when the spring has ground contact (Blickhan, 1989). We speculated that the third harmonic might be related, not only to asymmetry during ground contact but also to asymmetry during the suspension phase.

We also showed that modelling dFz_{peak} with acceleration features resulted in the best fits. The reason for this can possibly be explained by studying equation (10), which shows that the position (a_{xn}) and acceleration ($\widehat{a}_{xn}$) amplitudes are not proportional as the stride frequency (ω) is variable. Assuming a simple spring-mass model, dFz_{peak} should be proportional to $\widehat{a}_{x1}$.

Putting together the observations of the head, withers and pelvis coefficients (models C_{1f}, C_{1h}) explained how the timing of asymmetry was related to dFz_{peak}. For a hindlimb lameness, the horse could use its head and neck as a lever arm attached to the withers to shift weight diagonally forward, simultaneously keeping dFz_{peakf} small. Similarly, for a forelimb lameness, withers and head movement could be used when increasing dFz_{peakf} and shifting weight towards the diagonal hindlimb. This confirmed previously published results describing how neck and trunk torques were used to shift weight diagonally during induced forelimb lameness (Vorstenbosch et al., 1997). But also, how the late-step timing of pelvic asymmetry can appear to indicate the opposite

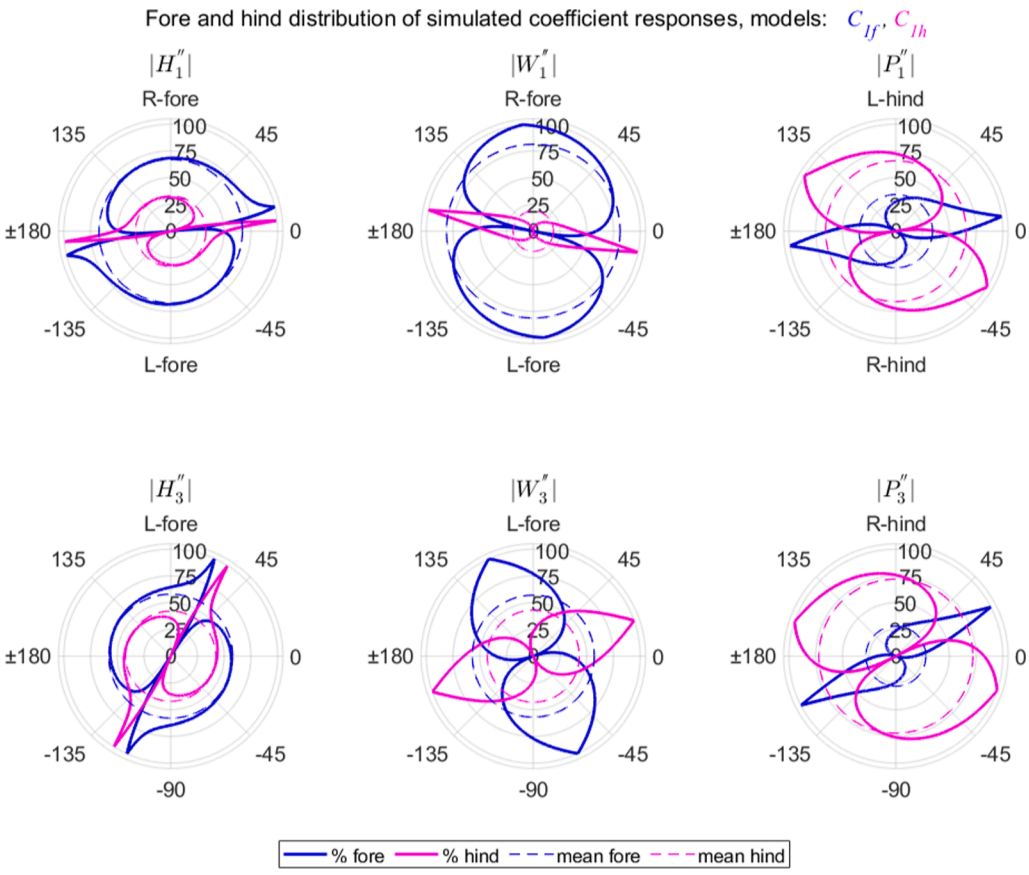

Fig. 4. Percent of fore and hind contributions to dFz_{peakf}(blue) and dFz_{peakh}(magenta) from the simulated coefficient responses for models C_{1f} and C_{1h}. Percent of response for component 1 (top) and 3 (bottom) are shown for head (H), withers (W) and pelvis (P). The mean contribution to dFz_{peakf} and dFz_{peakh}, taken over all possible phases, are indicated by the dashed lines. The approximate time of midstance for each limb is indicated along the phase axis. Note the different phase ranges where either the fore- or hindlimb models contribute the most to dFz_{peak}.

lame limb to the dFz_{peakh} and that the withers could be used to distinguish between primary fore- and hindlimb lameness (Kelmer et al., 2005; Rhodin et al., 2018). Standardised feature values and movement curves for the two examples in Fig. 1 are shown in Fig. 5 and Fig. 6.

4.2. Linear regression

Due to the complexity of the kinematics (timing, harmonic components, the interactions between trajectories) on the modelled dFz_{peak}, it would be difficult to consolidate this information into concise results manually. The regression models provided synthesised dFz_{peak} values that are easier to interpret. Evaluating whether the models provided sufficiently high accuracy was more difficult. Research on the correlation between subjective lameness grading and kinetic gait variables vary considerably.

Two studies, with horses trotted on a treadmill with induced lameness, reported the mean ± SD dFz_{peak} for subtle cases as, dFz_{peakf} : 1.4 ± 1.35% and dFz_{peakh} : 1.0 ± 1.15% and for mild cases as, dFz_{peakf} : 4.35 ± 2.35% and dFz_{peakh} : 3.75 ± 1.5% (Weishaupt et al., 2006, 2004). Note that the dFz_{peak} from Weishaupt et al., have been divided by two here to match our definition. Another treadmill study also showed considerable overlap in dFz_{peaks} for subtle and mild lameness' (Müller-Quirin et al., 2020). In a study where horses were induced with forelimb lameness and trotted over force plates, there was approximately a 7% decrease in forelimb Fz_{peak} (Δ%) per 0.5 AAEP lameness grade, as stated by Keegan, 2007 (Ishihara et al., 2005). Under the assumption that the sound contralateral limb Fz_{peak} does not change with lameness (Weishaupt et al., 2006), this translated to our force differences as, $dFz_{peak} = \frac{\Delta\%}{200-\Delta\%}$*100, which meant AAEP grades 0.5/1/1.5/2 corresponded to 3.6/7.5/11.7/16.3% dFz_{peakf}. When comparing the results from Weishaupt et al., 2006 and Ishihara et al., 2005 it is essential to clarify the methodological differences, i.e., treadmill vs overground and the potential disparity between grading scales. Regardless, our best regression models should still be able to reliably pick the correct limb and discriminate between grades in mild to severe weight-bearing lameness, based on our reported model RMSEs. The consolidation of fore- and hindlimb models enables evaluation of single limb, ipsilateral and contralateral weight-bearing asymmetry. It also provides a possible framework for explaining how horses can move asymmetrically but still have symmetric weight-bearing, e.g., theoretically, a horse could time its VMA to have minimal contributions towards dFz_{peak}, or have the contributions from head, withers and pelvis components cancel each other out. Identifying VMA that are not caused by a dFz_{peak} could provide the means to describe non-weight-bearing lamenesses. The small difference in predictive accuracy between the harmonic component models and the $D_{min/max}$ models make it hard to argue whether there is any benefit in picking one over the other. However, one advantage of using harmonic components is that even in the case of a severe asymmetry, where the minima and maxima are not discernible, features can still be extracted.

5. Limitations

The instrumented treadmill used in the study provided a controlled and consistent study environment, hence the validity of the results for over-ground movement and other surfaces was not ensured. Another restriction was that the treadmill did not measure horizontal forces and thus, these were not investigated. There has previously been shown a correlation between PD_{max} and hindlimb horizontal forces (Bell et al., 2016). A variety of breeds were included in the study (the majority being Warmblood riding horses), but breeds with potential differing gait strategies e.g., Icelandic horses, were not included in sufficient numbers to elucidate breed differences. Studying only dFz_{peak} did not enable the

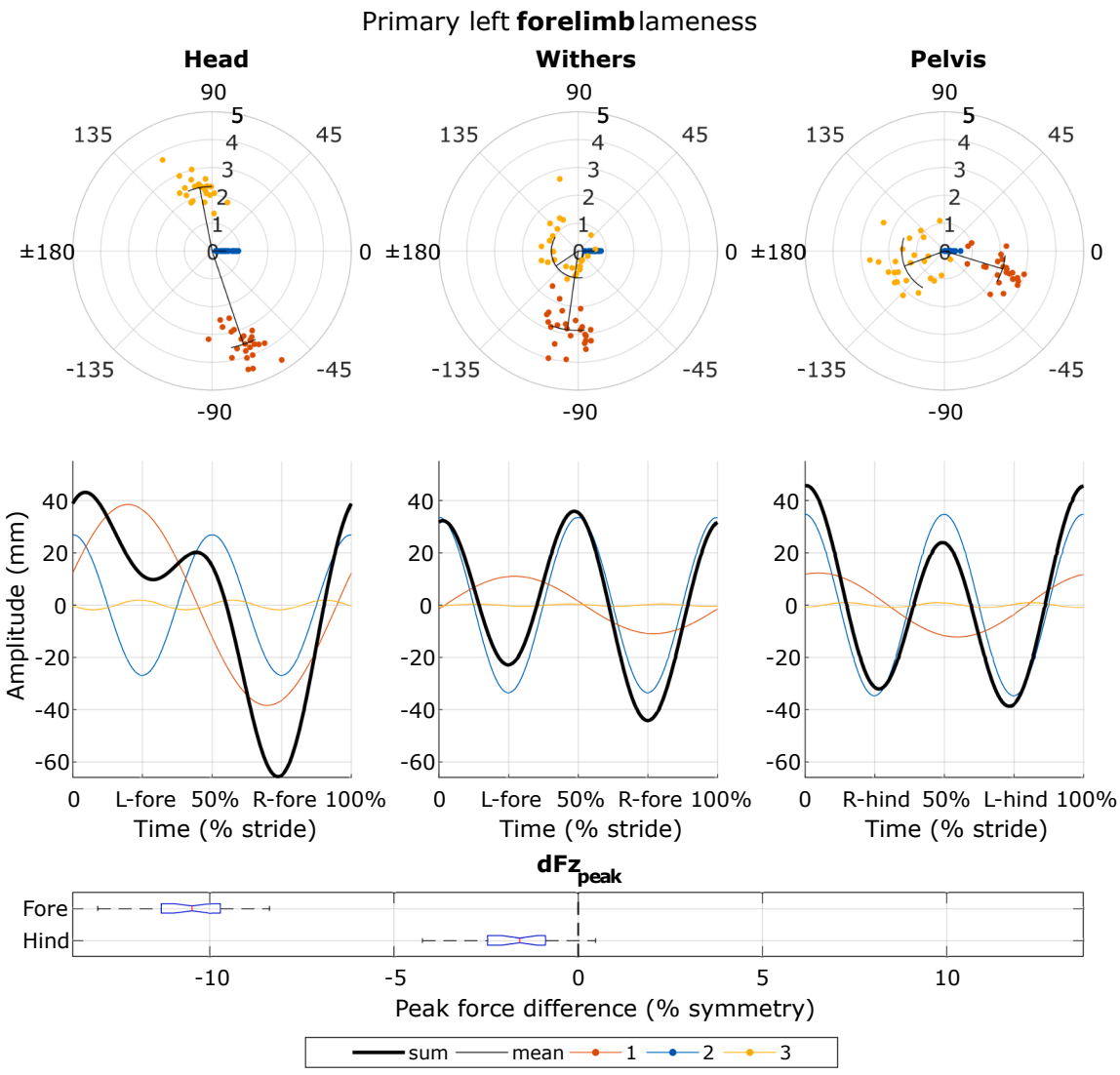

Fig. 5. Example of an induced left forelimb lameness. Standardised values of the first (1), second (2) and third (3) harmonic component are illustrated in the polar plots (top). The standardisation was made by first subtracting the mean value and then dividing by the standard deviation for each variable. The straight black lines indicate mean amplitude and phase of the components and the curved lines indicate the phase's standard deviation. The mean stride synthetisations of the components are shown below together with their superposition. Finally, the peak vertical force differences (dFz_{peak}) for the fore and hindlimbs are shown in the boxplots. Note the kinematic pelvis asymmetry which appears to indicate a right hind problem and the contradicting dFz_{peakh} indicating a left hind weight-bearing deficit.

quantification of bilateral lameness.

6. Conclusion

The interaction between kinematics and kinetics was shown to be complex and highly reliant not only on the VMA amplitude but also on the timing (phase) of the VMA, leading to the conclusion that the horse can use a multitude of different compensatory movement patterns, all with similar weight-bearing asymmetry. If the purpose of studying upper body VMA is to evaluate weight-bearing lameness, it is likely challenging for a human to synthesise all the relevant variables. The regression models proposed in this study appeared to provide sufficient accuracy for clinical use. dFz_{peak} predictions, together with the knowledge of typical compensatory mechanisms, can enable the quantification of single limb, ipsilateral and contralateral weight-bearing lameness.

Including kinematic asymmetry from the head, withers and pelvis, when modelling dFz_{peak} produced significantly better fits than when withers asymmetry was excluded or when using head and pelvis asymmetry in individual models. The effect was more pronounced for dFz_{peakf} than for dFz_{peakh}. Including information from the third harmonic component and using acceleration VMA further significantly improved the fit and prediction accuracy of dFz_{peak}, though the practical significance of this improved accuracy could not be concluded. Future studies need to address clinical and over-ground validation on different surfaces as well as evaluating different gaits. Non-linear machine learning methods could potentially improve dFz_{peak} predictions.

CRediT authorship contribution statement

Christoffer Roepstorff: Writing – original draft, Software, Methodology, Investigation, Formal analysis, Data curation, Conceptualization. **Annik Imogen Gmel:** Writing - review & editing, Investigation, Funding acquisition. **Samuel Arpagaus:** Software, Investigation, Data curation. **Filipe Manuel Serra Bragança:** Investigation, Software. **Elin Hernlund:** Investigation. **Lars Roepstorff:** Investigation. **Marie Rhodin:** Investigation, Funding acquisition. **Michael Andreas Weishaupt:** Supervision, Investigation.

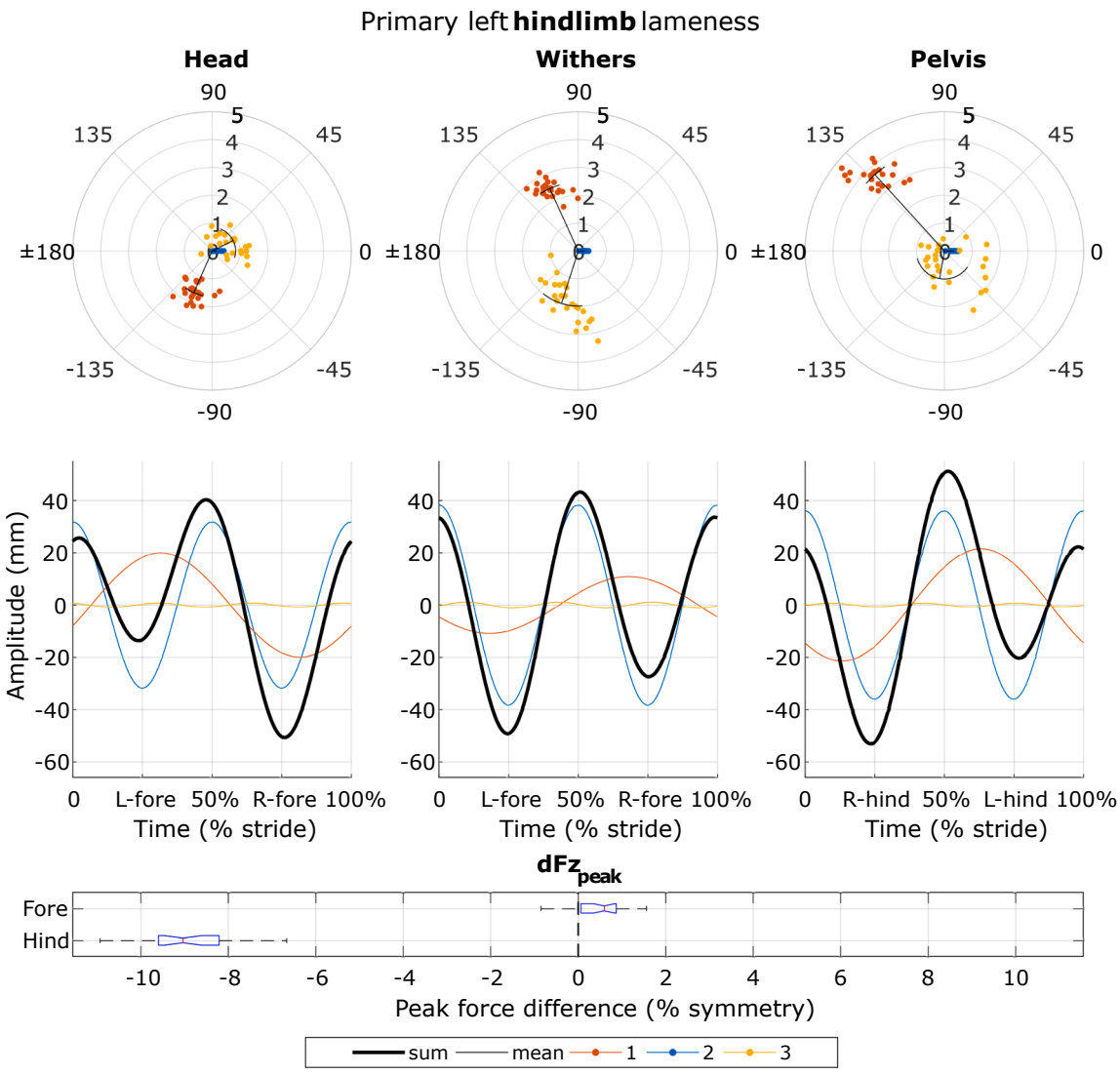

Fig. 6. Example of an induced left hindlimb lameness. Standardised values of the first (1), second (2) and third (3) harmonic component are illustrated in the polar plots (top). The standardisation was made by first subtracting the mean value and then dividing by the standard deviation for each variable. The straight black lines indicate mean amplitude and phase of the components and the curved lines indicate the phase's standard deviation. The mean stride synthetisations of the components are shown below together with their superposition. Finally, the peak vertical force differences (dFz_{peak}) for the fore and hindlimbs are shown in the boxplots. Note that the head and withers asymmetry are indicating opposite limb problems and the almost symmetric dFz_{peakf}.

Declaration of Competing Interest

The Ph.D. of C.R was partially financed by Qualisys AB, Sweden. The authors declare that they have no other known competing financial interests or personal relationships that could have appeared to influence the work reported in this paper.

Acknowledgements

A.I.G was financed by the Swiss Federal Office for Agriculture, # 625000469. The project P1 was financed by Swedish-Norwegian Foundation for Equine Research (H1247074). M.R was financed by Marie-Claire Cronstedts Stiftelse, Sweden. Matthias Haab for the drawings.

Appendix A. Supplementary data

Supplementary data to this article can be found online at https://doi.org/10.1016/j.jbiomech.2022.111097.

References

Audigié, F., Pourcelot, P., Degueurce, C., Geiger, D., Denoix, J.M., 2002. Fourier analysis of trunk displacements: A method to identify the lame limb in trotting horses. J. Biomech. 35 (9), 1173–1182. https://doi.org/10.1016/S0021-9290(02)00089-1.

Bell, R.P., Reed, S.K., Schoonover, M.J., Whitfield, C.T., Yonezawa, Y., Maki, H., Pai, P.F., Keegan, K.G., 2016. Associations of force plate and body-mounted inertial sensor measurements for identification of hind limb lameness in horses. Associations of force plate and body-mounted inertial sensor measurements for identification of hind limb lameness in horses. 77 (4), 337–345.

Belsley, D.A., Kuh, E., Welsch, R.E., 1980. Regression Diagnostics, Ecosystems (New York, N.y.), Wiley Series in Probability and Statistics. John Wiley & Sons, Inc., Hoboken, NJ, USA. Doi: 10.1002/0471725153.

Berens, P., 2015. CircStat : A MATLAB Toolbox for Circular Statistics. J. Stat. Softw. 31, 1–21. https://doi.org/10.18637/jss.v031.i10.

Blickhan, R., 1989. The spring-mass model for running and hopping. J. Biomech. 22 (11-12), 1217–1227. https://doi.org/10.1016/0021-9290(89)90224-8.

Bosch, S., Serra Bragança, F., Marin-Perianu, M., Marin-Perianu, R., van der Zwaag, B., Voskamp, J., Back, W., van Weeren, R., Havinga, P., Bosch, S., Serra Bragança, F., Marin-Perianu, M., Marin-Perianu, R., van der Zwaag, B.J., Voskamp, J., Back, W., van Weeren, R., Havinga, P., 2018. EquiMoves: A Wireless Networked Inertial Measurement System for Objective Examination of Horse Gait. Sensors 18, 850. https://doi.org/10.3390/s18030850.

Buchner, H.H.F., Savelberg, H.H.C.M., Schamhardt, H.C., Barneveld, A., 1996. Head and trunk movement adaptations in horses with experimentally induced fore- or

hindlimb lameness. Equine Vet. J. 28, 71–76. https://doi.org/10.1111/j.2042-3306.1996.tb01592.x.

Halling Thomsen, M., Tolver Jensen, A., Sørensen, H., Lindegaard, C., Haubro Andersen, P., 2010. Symmetry indices based on accelerometric data in trotting horses. J. Biomech. 43 (13), 2608–2612. https://doi.org/10.1016/j.jbiomech.2010.05.004.

Ishihara, A., Bertone, A.L., Rajala-Schultz, P.J., 2005. Association between subjective lameness grade and kinetic gait parameters in horses with experimentally induced forelimb lameness. Am. J. Vet. Res. 66 (10), 1805–1815. https://doi.org/10.2460/ajvr.2005.66.1805.

Keegan, K.G., 2007. Evidence-Based Lameness Detection and Quantification. Veterinary Clinics of North America: Equine Practice 23 (2), 403–423.

Keegan, K.G., Wilson, D.A., Smith, B.K., Wilson, D.J., 2000. Changes in kinematic variables observed during pressure-induced forelimb lameness in adult horses trotting on a treadmill. Am. J. Vet. Res. 61 (6), 612–619. https://doi.org/10.2460/ajvr.2000.61.612.

Kelmer, G., Keegan, K.G., Kramer, J., Wilson, D.A., Pai, F.P., Singh, P., 2005. Computer-assisted kinematic evaluation of induced compensatory movements resembling lameness in horses trotting on a treadmill. Am. J. Vet. Res. 66 (4), 646–655. https://doi.org/10.2460/ajvr.2005.66.646.

Kramer, J., Keegan, K.G., Wilson, D.A., Smith, B.K., Wilson, D.J., 2000. Kinematics of the hind limb in trotting horses after induced lameness of the distal intertarsal and tarsometatarsal joints and intra-articular administration of anesthetic. Am. J. Vet. Res. 61 (9), 1031–1036. https://doi.org/10.2460/ajvr.2000.61.1031.

Merkens, H.W., Schamhardt, H.C., 1988a. Evaluation of equine locomotion during different degrees of experimentally induced lameness I: Lameness model and quantification of ground reaction force patterns of the limbs. Equine Vet. J. 20, 99–106. https://doi.org/10.1111/j.2042-3306.1988.tb04655.x.

Merkens, H.W., Schamhardt, H.C., 1988b. Evaluation of equine locomotion during different degrees of experimentally induced lameness II: Distribution of ground reaction force patterns of the concurrently loaded limbs. Equine Vet. J. 20, 107–112. https://doi.org/10.1111/j.2042-3306.1988.tb04656.x.

Müller-Quirin, J., Dittmann, M.T., Roepstorff, C., Arpagaus, S., Latif, S.N., Weishaupt, M. A., 2020. Riding Soundness—Comparison of Subjective With Objective Lameness Assessments of Owner-Sound Horses at Trot on a Treadmill. Journal of Equine Veterinary Science 95, 103314. https://doi.org/10.1016/j.jevs.2020.103314.

Peham, C., Scheidl, M., Licka, T., 1996. A method of signal processing in motion analysis of the trotting horse. J. Biomech. 29 (8), 1111–1114. https://doi.org/10.1016/0021-9290(95)00179-4.

Peloso, J.G., Stick, J.A., Soutas-Little, R.W., Caron, J.C., DeCamp, C.E., Leach, D.H., 1993. Computer-assisted three-dimensional gait analysis of amphotericin-induced carpal lameness in horses. Am. J. Vet. Res. 54, 1535–1543.

Rhodin, M., Persson-Sjodin, E., Egenvall, A., Serra Bragança, F.M., Pfau, T., Roepstorff, L., Weishaupt, M.A., Thomsen, M.H., van Weeren, P.R., Hernlund, E., 2018. Vertical movement symmetry of the withers in horses with induced forelimb and hindlimb lameness at trot. Equine Vet. J. 50 (6), 818–824. https://doi.org/10.1111/evj.12844.

Roepstorff, C., Dittmann, M.T., Arpagaus, S., Serra Bragança, F.M., Hardeman, A., Persson-Sjödin, E., Roepstorff, L., Gmel, A.I., Weishaupt, M.A., 2021. Reliable and clinically applicable gait event classification using upper body motion in walking and trotting horses. J. Biomech. 114, 110146. https://doi.org/10.1016/j.jbiomech.2020.110146.

Serra Bragança, F.M., Hernlund, E., Thomsen, M.H., Waldern, N.M., Rhodin, M., Byström, A., Weeren, P.R., Weishaupt, M.A., 2021. Adaptation strategies of horses with induced forelimb lameness walking on a treadmill. Equine Veterinary Journal evj.13344. 53 (3), 600–611. https://doi.org/10.1111/evj.13344.

Serra Bragança, F.M., Rhodin, M., van Weeren, P.R., 2018. On the brink of daily clinical application of objective gait analysis: What evidence do we have so far from studies using an induced lameness model? Veterinary Journal 234, 11–23. https://doi.org/10.1016/j.tvjl.2018.01.006.

Serra Bragança, F.M., Roepstorff, C., Rhodin, M., Pfau, T., van Weeren, P.R., Roepstorff, L., 2020. Quantitative lameness assessment in the horse based on upper body movement symmetry: The effect of different filtering techniques on the quantification of motion symmetry. Biomed. Signal Process. Control 57, 101674. https://doi.org/10.1016/j.bspc.2019.101674.

Sonnberger, H., 1989. Regression diagnostics: Identifying influential data and sources of collinearity, by D. A. Belsley, K. Kuh and R. E. Welsch. (John Wiley & Sons, New York, 1980, pp. xv + 292, ISBN 0-471-05856-4, cloth $39.95. Journal of Applied Econometrics 4, 97–99. Doi: 10.1002/jae.3950040108.

Uhlir, C., Licka, T., Kübber, P., Peham, C., Scheidl, M., Girtler, D., 1997. Compensatory movements of horses with a stance phase lameness. Equine Vet. J. 29, 102–105. https://doi.org/10.1111/j.2042-3306.1997.tb05065.x.

Vorstenbosch, M.A.T.M., Buchner, H.H.F., Savelberg, H.H.C.M., Schamhardt, H.C., Barneveld, A., 1997. Modeling study of compensatory head movements in lame horses. Am. J. Vet. Res. 58, 713–718.

Weishaupt, M.A., Hogg, H.P., Wiestner, T., Denoth, J., Stussi, E., Auer, J.A., 2002. Instrumented treadmill for measuring vertical ground reaction forces in horses. Am. J. Vet. Res. 63 (4), 520–527. https://doi.org/10.2460/ajvr.2002.63.520.

Weishaupt, M.A., Wiestner, T., Hogg, H.P., Jordan, P., Auer, J.A., 2006. Compensatory load redistribution of horses with induced weight-bearing forelimb lameness trotting on a treadmill. Veterinary Journal 171 (1), 135–146. https://doi.org/10.1016/j.tvjl.2004.09.004.

Weishaupt, M.A., Wiestner, T., Hogg, H.P., Jordan, P., Auer, J.A., 2004. Compensatory load redistribution of horses with induced weightbearing hindlimb lameness trotting on a treadmill. Equine Vet. J. 36, 727–733. https://doi.org/10.2746/0425164044848244.